Supplementary Materials for

Convective transition statistics over tropical oceans for climate model diagnostics: Observational baseline

Yi-Hung Kuo, * Kathleen A. Schiro, and J. David Neelin

Department of Atmospheric and Oceanic Sciences, University of California Los Angeles, Los Angeles, CA, USA

Content of this file

S1. Gap-filling methods for TMIv7.1 CWV

S2. Bulk measures of tropospheric temperature

S3. Estimating critical CWV

S4. Sensitivity of convective transition statistics (and their spatial-resolution-dependence) to gap-filling

S5. Joint-PDF of CWV relative to critical and precipitation for different temperature and basin

S6. Geographic distribution of bulk tropospheric temperature

S7. CWV relative to critical as an indicator of precipitation

S8. Low bias of conditional precipitation associated with ground-based CWV measurements

S1. Gap-filling methods for TMIv7.1 CWV

The latest algorithm (version 7.1) adopted by the Remote Sensing Systems (RSS; Wentz et al. 2015) for column-integrated water vapor (CWV) and precipitation retrievals occasionally does not return a CWV value in the presence of precipitation. Figure S1 shows an example of this (chosen to illustrate a severe case, as opposed to a typical situation). One may note that regions with missing CWV, as indicated by black in the upper panel, coincide with regions of high precipitation, as indicated by warm colors in the lower panel.

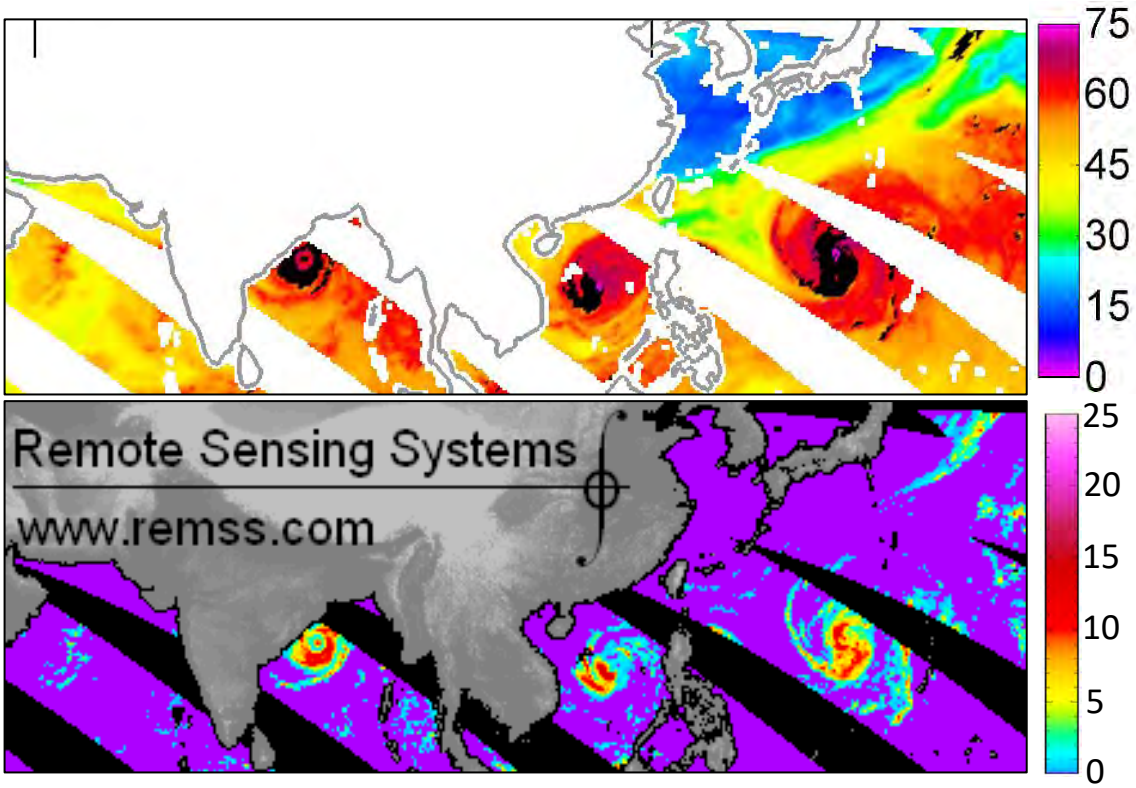

Figure S1: TMIv7.1 CWV (upper; units: mm) and precipitation rate (lower; units: mm hr^{-1}) for TRMM descending passes on 12 October 2013. In the upper panel, regions of missing CWV are shown by black. The image in the lower panel is directly downloaded from the RSS website. The three tropical cyclones, from left to right, are Phailin, Nari, and Wipha.

The probability of missing CWV is shown in Fig. S2. The probability depends primarily on precipitation rate and shows little sensitivity to bulk tropospheric temperature and basin. There is also no noticeable annual variability (not shown). Because the missing values are associated with higher precipitation, the raw TMIv7.1 data product has significant biases. This applies even to the climatology, for instance, when precipitation values without CWV retrievals are excluded, the annual mean precipitation rate over tropical oceans calculated using the TMIv7.1 data is reduced from ~ 3.1 to ~ 2.1 mm hr^{-1}. As such, it is necessary to gap-fill the missing CWV values to avoid distortion of the desired precipitation-CWV relation.

Three gap-filling methods are tested. The first approach fills the missing values using the available CWV value at the geographically nearest pixel. When there are multiple such pixels, the maximum

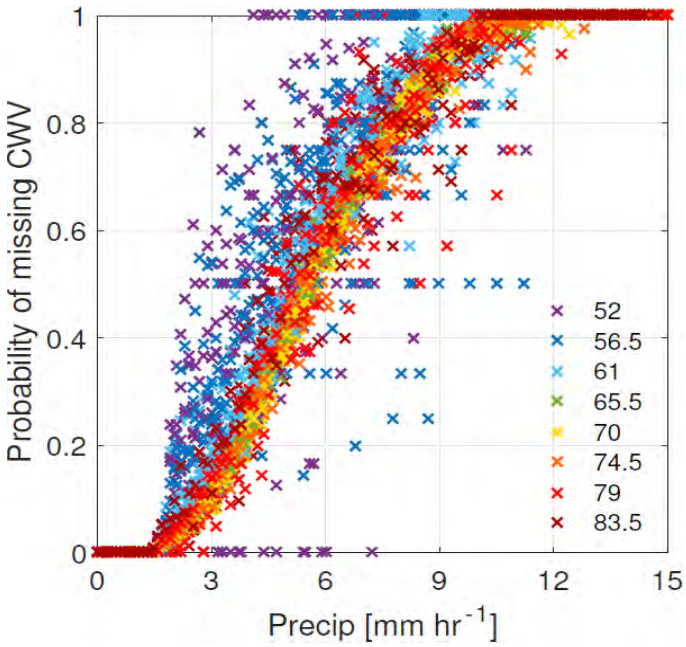

Figure S2: Probability of missing CWV as a function of precipitation rate and $\widehat{q_{sat}}$ (colors; units: mm) for four tropical ocean basins calculated using TMIv7.1 CWV and precipitation, and Reanalysis-2 temperature for 2005.

among the available CWV values is used. This method, referred to as "Nearest" here, is our default choice for CWV gap-filling. The second approach starts with identifying "holes" of missing CWV. For all pixels in each hole, we then fill missing values with the maximum CWV value on the circumference. This approach is referred to as "Max." The third method, "Mean," is similar to Max, but uses a mean instead. Among these three methods, Max assigns more high CWV values, and Mean assigns less high CWV values, while Nearest lies somewhere in between. A fourth method based on biharmonic spline interpolation provided by MATLAB (see https://www.mathworks.com/help/matlab/ref/griddata.html; option 'v4') has also been tested; the results are similar to Max, and hence is not presented here.

The sensitivity of the convective transition statistics (and their spatial-resolution dependence) to gap-filling is discussed in Section S4 (Figs. S7-S11).

S2. Bulk measures of tropospheric temperature

In the presence of convection, the tropospheric temperature tends to exhibit vertically coherent structure (as in Fig. 4 of the main text). Therefore, bulk measures of tropospheric temperature, such as the column-integrated saturation humidity $\widehat{q_{sat}}$ (units: mm) and mass-weighted column average temperature $\hat{T}$ (units: K) are expected to be useful in characterizing convection, and different bulk measures are expected to yield similar characterization. To verify this assertion directly, Fig. S3 shows that the joint-PDF of $\widehat{q_{sat}}$ and $\hat{T}$ over tropical oceans are clearly well-correlated.

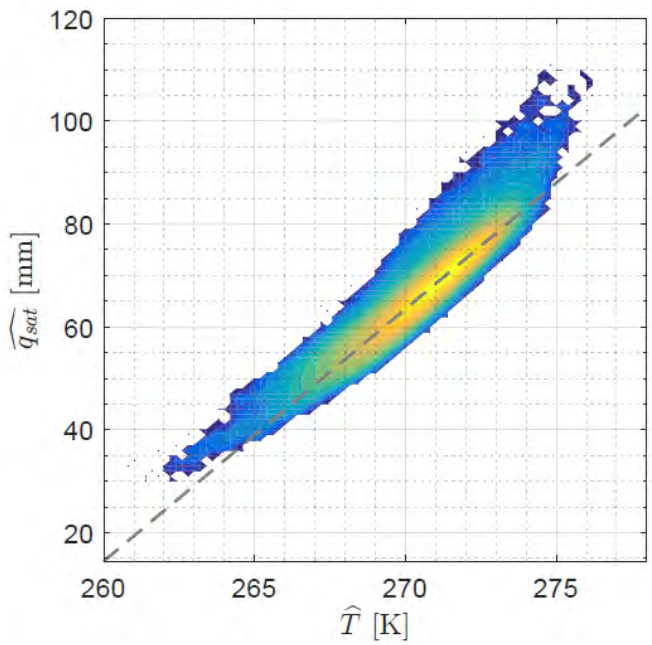

Figure S3: Joint-PDF ($\log_{10}$) of $\widehat{q_{sat}}$ and $\hat{T}$ over tropical oceans calculated using Reanalysis-2 temperature for 2005. The color advances when the values of the joint-PDF doubles ($10^{0.3}$ ~ 2). The gray dashed line represents the linear regression with slope ~ 4.9 mm K^{-1}.

Figure 1 in the main text shows the convective transition statistics conditioned on $\widehat{q_{sat}}$. The corresponding statistics conditioned on $\hat{T}$ are shown in Fig. S4. As expected, statistics in these two figures demonstrate similar behaviors.

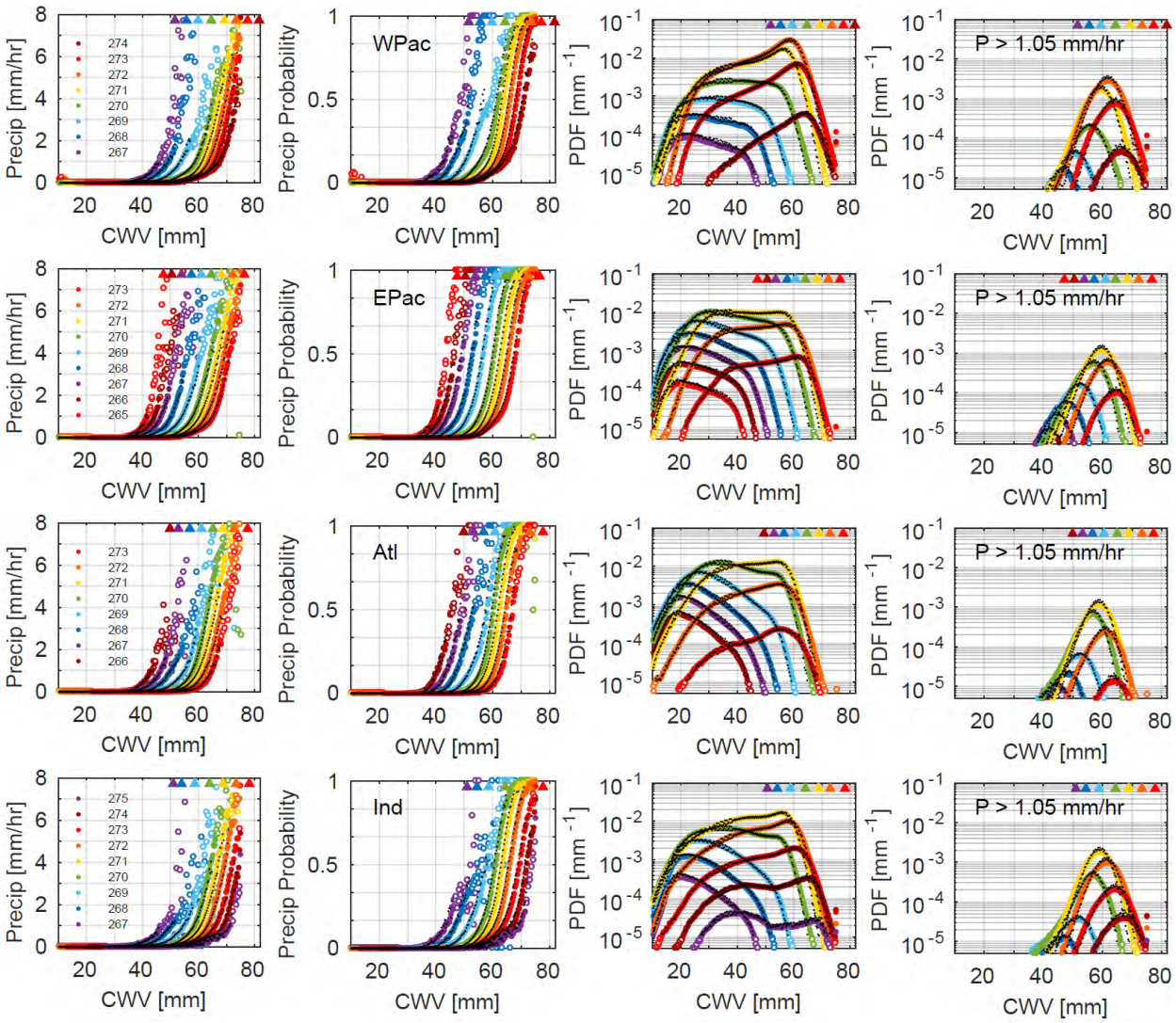

Figure S4: Similar to Fig. 1 of the main text but conditioned on $\hat{T}$ instead of $\widehat{q_{sat}}$ as the measure of tropospheric temperature. Conditionally averaged precipitation rate (1st col. from left), conditional probability of precipitation (2nd col.), probability density function of all events (3rd col.) and precipitating events only (4th col.) as a function of CWV and $\hat{T}$ (units: K) for four tropical ocean basins (20°S-20°N): western Pacific (WPac; 1st row), eastern Pacific (EPac; 2nd row), Atlantic (Atl; 3rd row), and Indian Ocean (Ind; 4th row). Results are shown using TMIv7.1 data and Reanalysis-2 temperature for the period of 01 Jun 2002 – 31 May 2014 compiled at 0.25° (colored markers) and 0.5° (black dots). Underpopulated bins at 0.25° (PDF < 10^{-5}) are indicated by open circles, and those for 0.5° are omitted. Triangles represent the corresponding $\widehat{q_{sat}}$ values. Here, precipitating events are defined by P > 1.05 mm hr^{-1}. The CWV data is gap-filled using nearest available values, and data from pixels within 2.5° of land are excluded to avoid potentially erroneous temperature values arising from spatial interpolation.

S3. Estimating critical CWV

The critical CWV w_c is used to characterize the location of the strong increase in conditionally average precipitation and probability of precipitation, and related drops in probability of CWV. Here we detail how this is estimated from the statistics presented in Figs. 1 and S4. Throughout this study, we use the following estimator for w_c: the CWV value at which the asymptote of the conditional precipitation curve intersects with the CWV-axis, with the asymptote being approximated by the best-fit line of a segment of the precipitation pickup (recall Fig. 2 in the main text). In practice, the curves for some temperature bins may not reach the high precipitation regime so that their asymptotes (and hence the best-fit lines) are not sufficiently well-sampled for robust estimation. We thus work with the assumption that the precipitation pickup curves can be collapsed by shifting CWV by a suitable amount depending on the temperature, and the slope of the best-fit line does not depend strongly on temperature. One can refer to Figs. 2-3 in the main text, and Figs. S5-S11 below to assess the validity of this assumption.

Consider the case where $\widehat{q_{sat}}$ is used as the bulk temperature measure. We start with choosing a fixed reference precipitation rate P_r (say, 1.05 mm hr^{-1} as used here). For each $\widehat{q_{sat}}$, we can find the reference CWV w_r at which the conditional precipitation equals P_r. Having found $w_r(\widehat{q_{sat}})$, the assumption implies that the precipitation pickup curves can be collapsed by shifting CWV by $w_r(\widehat{q_{sat}})$ for each $\widehat{q_{sat}}$, i.e., expressing statistics as a function of $cwv - w_r(\widehat{q_{sat}})$ instead. After the curves collapse into a single cluster, one can then take a segment of the cluster with the precipitation rate falling within a certain range (here, $3 < P < 5$ mm hr^{-1}) to find the best-fit line and its (shifted) CWV-intercept. Note that the difference between $w_r(\widehat{q_{sat}})$ and $w_c(\widehat{q_{sat}})$ under this procedure is independent of $\widehat{q_{sat}}$, and is typically around 1.75 mm (given by P_r divided by the slope of the pickup curve, α). The value of w_r would correspond approximately to the measure of critical used in Sahany et al. (2014).

The critical values found by the procedure just outlined, and hence the resulting collapsed statistics, are reasonably insensitive to the reference P_r and the specified precipitation range. There are, however, occasions for which special care is necessary. An example of such occasion (but without the proper care for demonstration purposes) is shown in Figs. S8 and S11 below for the 274-K $\hat{T}$-bin in the tropical western Pacific (WPac). In this case, the conditional precipitation as a function of CWV (gap-filled by Mean) has an irregular behavior for precipitation rate around P_r, leading to a w_r sensitive to P_r, and hence an unsatisfactory collapse. In this particular case, a set of carefully chosen P_r (and precipitation range in some other cases) can resolve the issue. There are, however, cases where the precipitation pickup is too irregular compared with observation (e.g., non-monotonic as a function of CWV) and the procedure outlined above would simply fail (e.g., output from a model with ill-constrained convective parameterization; not shown).

Note that in some of the figures presenting the collapsed statistics, the colored markers and black dots represent statistics compiled at different resolutions using the same gap-filling method (Figs. 2, S5, S6, and S9-S11), respectively, and represent statistics using different gap-filling at the same resolution in the others (Figs. S7-S8). Figures S5-S6 show the same statistics as in Fig. 2 in the main text, but include other basins. In all of these figures, the black-dot statistics are collapsed by using the critical values calculated for the colored-marker statistics. Since the lower-resolution conditional precipitation usually does not reach the high precipitation regime, this approach enables us to collapse the lower-resolution (black-dot) statistics without choosing a different range of precipitation, and still leads to a satisfactory collapse. One can assess this last assertion, and the sensitivity of the critical values and the collapsed

statistics to the resolution/gap-filling as indicated by the differences between the color-marker and black-dot statistics, by referring to these figures (with the exception of the 274-K $\hat{T}$-bin for WPac in Fig. S8).

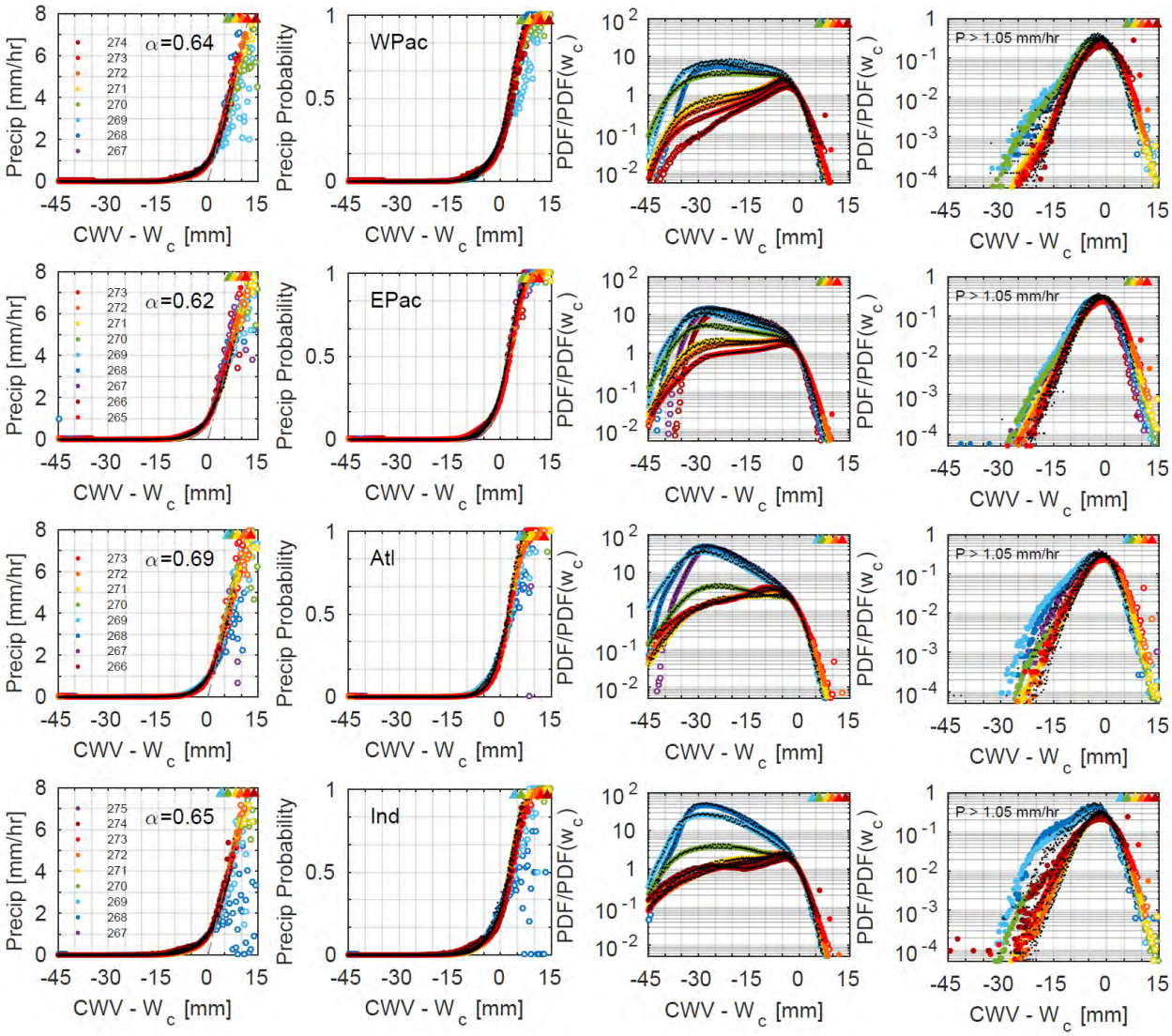

Figure S5: Convective transition statistics for each ocean basin, as in Fig. S4 for 0.25° (colored markers) and 0.5° (dots), but for each $\hat{T}$ shifted by the corresponding critical CWV w_c (as in Fig. 3g), and with PDFs scaled. The best-fit lines for conditional precipitation rates (leftmost col.) are shown as gray dash-dot line, with slope indicated by α. The top row is identical to the bottom row in Fig. 2.

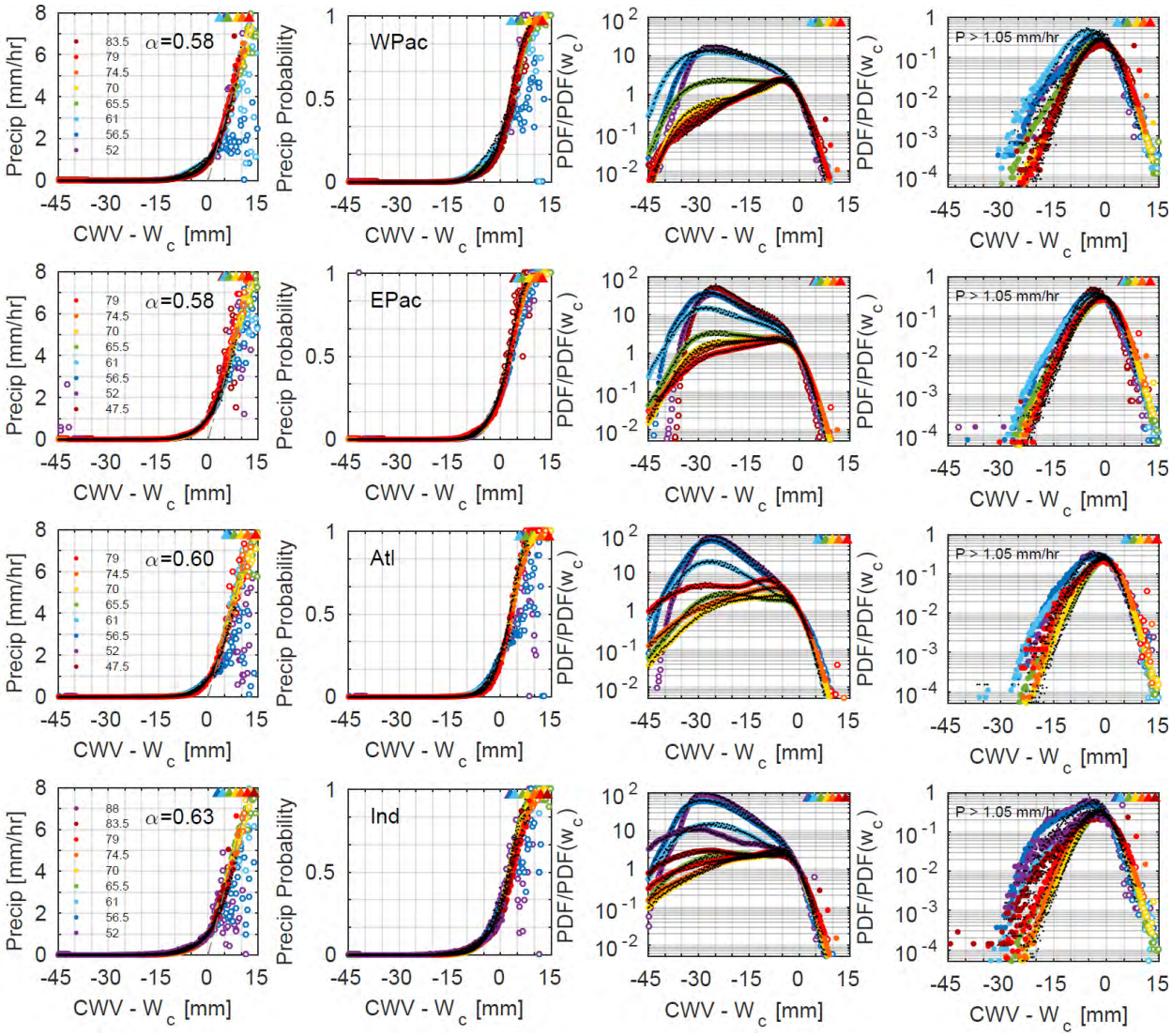

Figure S6: Same as Fig. S5, but conditionally averaged by $\widehat{q_{sat}}$ as in Fig. 1. The top row is identical to the top row in Fig. 2.

S4. Sensitivity of convective transition statistics (and their spatial-resolution-dependence) to gap-filling

In this section, we examine the sensitivity of the convective transition statistics (and their dependence on spatial-averaging) to the adopted gap-filling method. As mentioned in Section S3, in Figs. S7-S11, the black-dot statistics are collapsed by using the critical values calculated for the colored-marker statistics.

Figures S7 shows the (collapsed) statistics at 0.25° compiled using TMIv7.1 data with CWV gap-filled by Max (colored markers) and Nearest (default; black dots). The two methods lead to very similar results. Noticeable differences include the slope of the precipitation pickup and the PDF at high CWV — the former method results in a steeper pickup in terms of conditional precipitation and probability, and more frequent occurrences of CWV exceeding critical. Figure S8 is similar to Fig. S7, but with statistics for Max replaced by Mean. The latter method leads to a less steep precipitation pickup, and slightly less frequent occurrences of CWV above critical.

To further examine how the gap-filling method impacts the sensitivity of the statistics to spatial resolution, Figs. S9-S11 show the collapsed statistics compiled using TMIv7.1 CWV data gap-filled by Max (0.25° and 1.5°), Nearest (0.25° and 1°), and Mean (0.25° and 0.5°), respectively. The choices of resolution for Max and Nearest are the lowest resolution up to which a noticeable difference starts to appear. Here we should leave aside the conditional probability and PDF of precipitating events since they are expected to be sensitive to resolution. Max leads to the conditional precipitation most robust to spatial resolution, with the slope of the asymptote being almost invariant up to 1.5°, while Mean results in the least robust conditional precipitation and a noticeable reduction in the slope for 0.5° compared to 0.25°.

Overall, Max assigns more high CWV values and leads to statistics most robust to spatial-averaging, Mean is at the other end of the spectrum, and Nearest lies somewhere in between. For comparison purposes, Nearest is chosen as the default gap-filling method for this study. Although currently available observational datasets cannot provide sufficient information to favor one method over another, Yano et al. (2012) analyzed output from a cloud-resolving model (CRM) and concluded that the conditional precipitation as a function of CWV is indeed very robust to spatial-averaging. In light of the CRM study, our default choice of gap-filling may be too conservative, and Max leads to statistics more consistent with the CRM simulation in terms of being insensitive to spatial resolution.

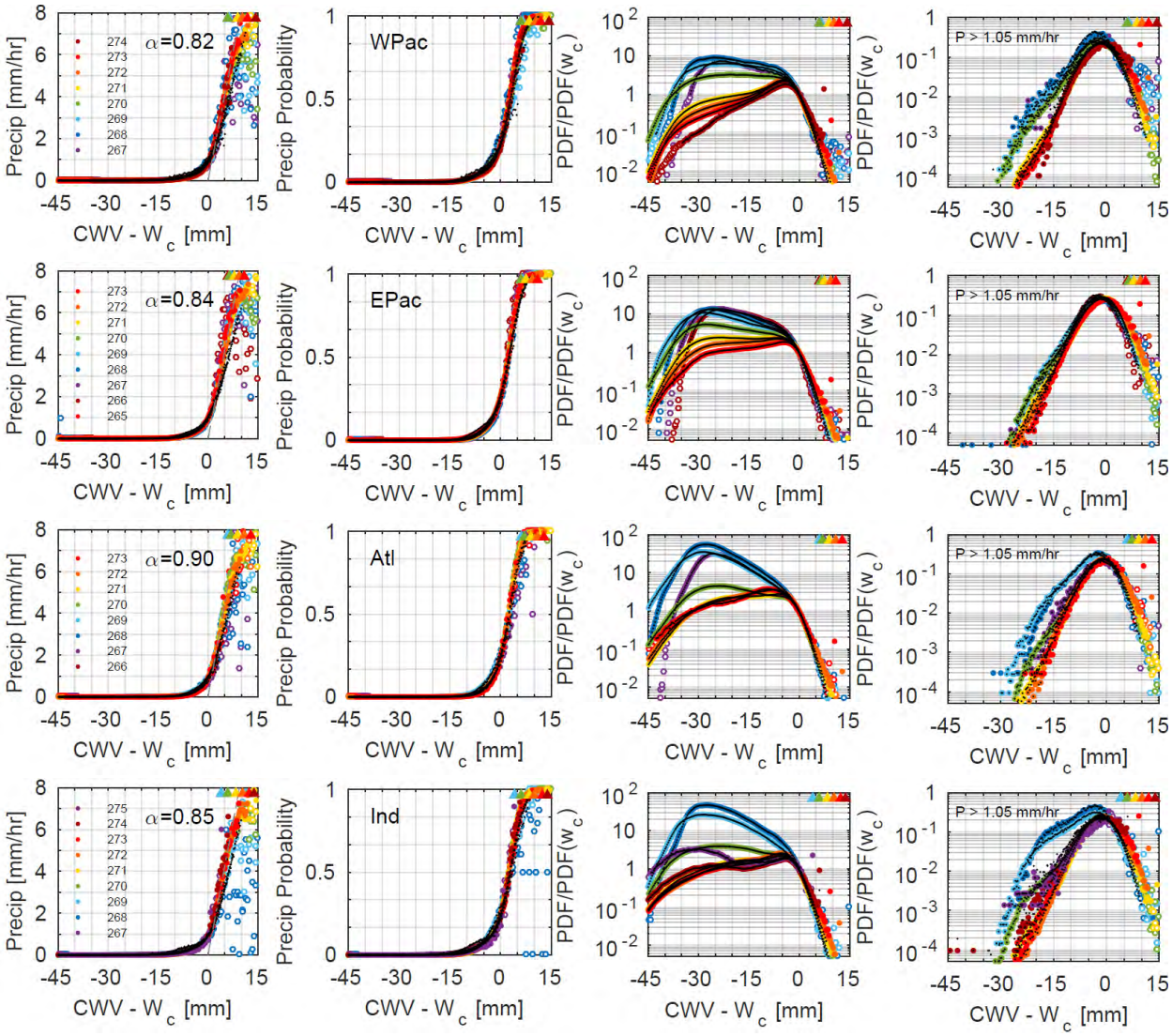

Figure S7: Convective transition statistics as in Fig. S4 for 0.25° (colored markers), but with CWV gap-filled using Max. The black dots are a duplication of the colored markers in Fig. S4 (the statistics for 0.25° with CWV gap-filled using Nearest).

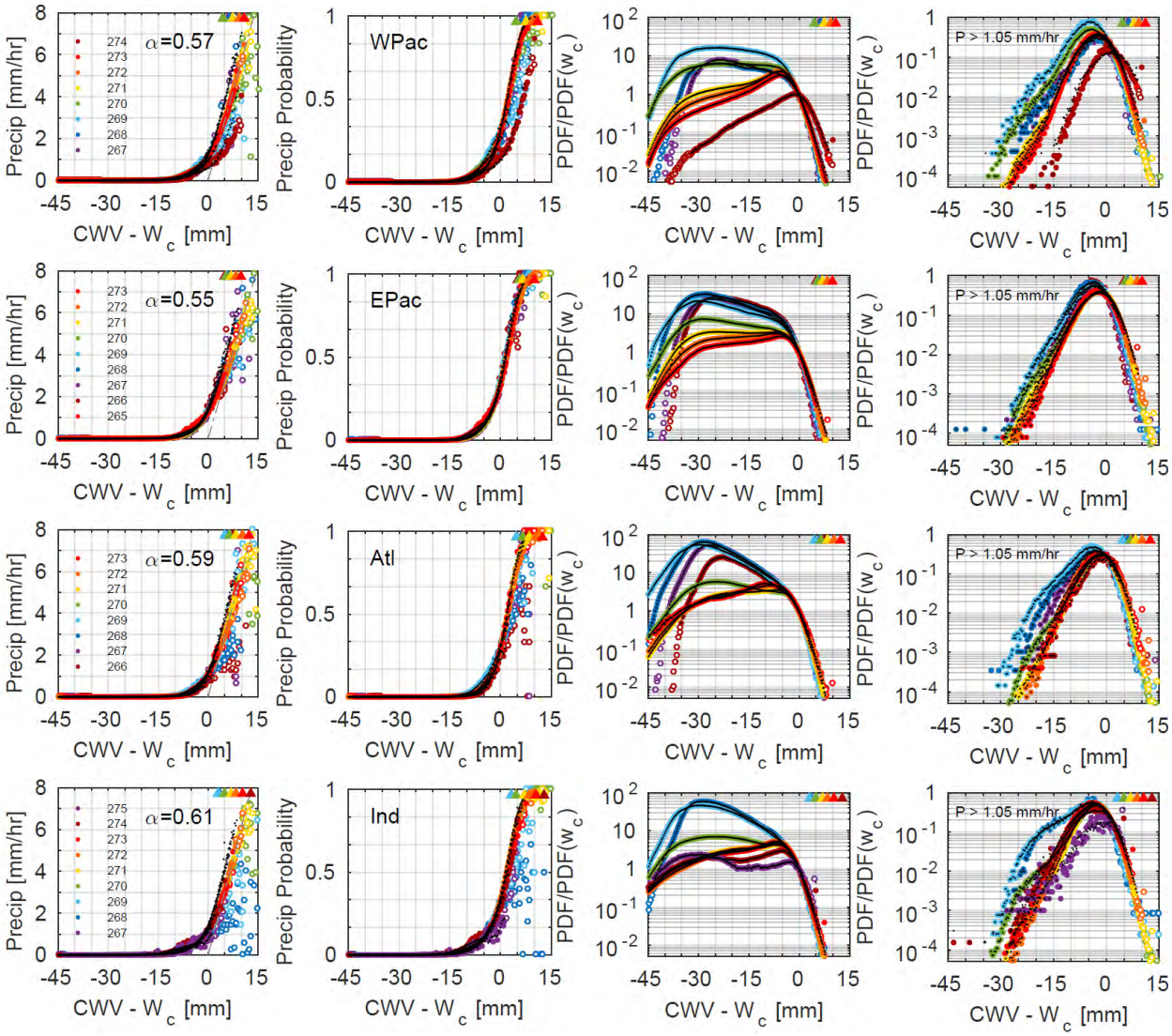

Figure S8: Convective transition statistics as in Fig. S4 for 0.25° (colored markers), but with CWV gap-filled using Mean. The black dots are a duplication of the colored markers in Fig. S4 (the statistics for 0.25° with CWV gap-filled using Nearest). The 274-K $\hat{T}$-bin for WPac requires the additional effort of choosing a larger P_r to collapse the statistics, which is not done here for illustration purpose (Section S3).

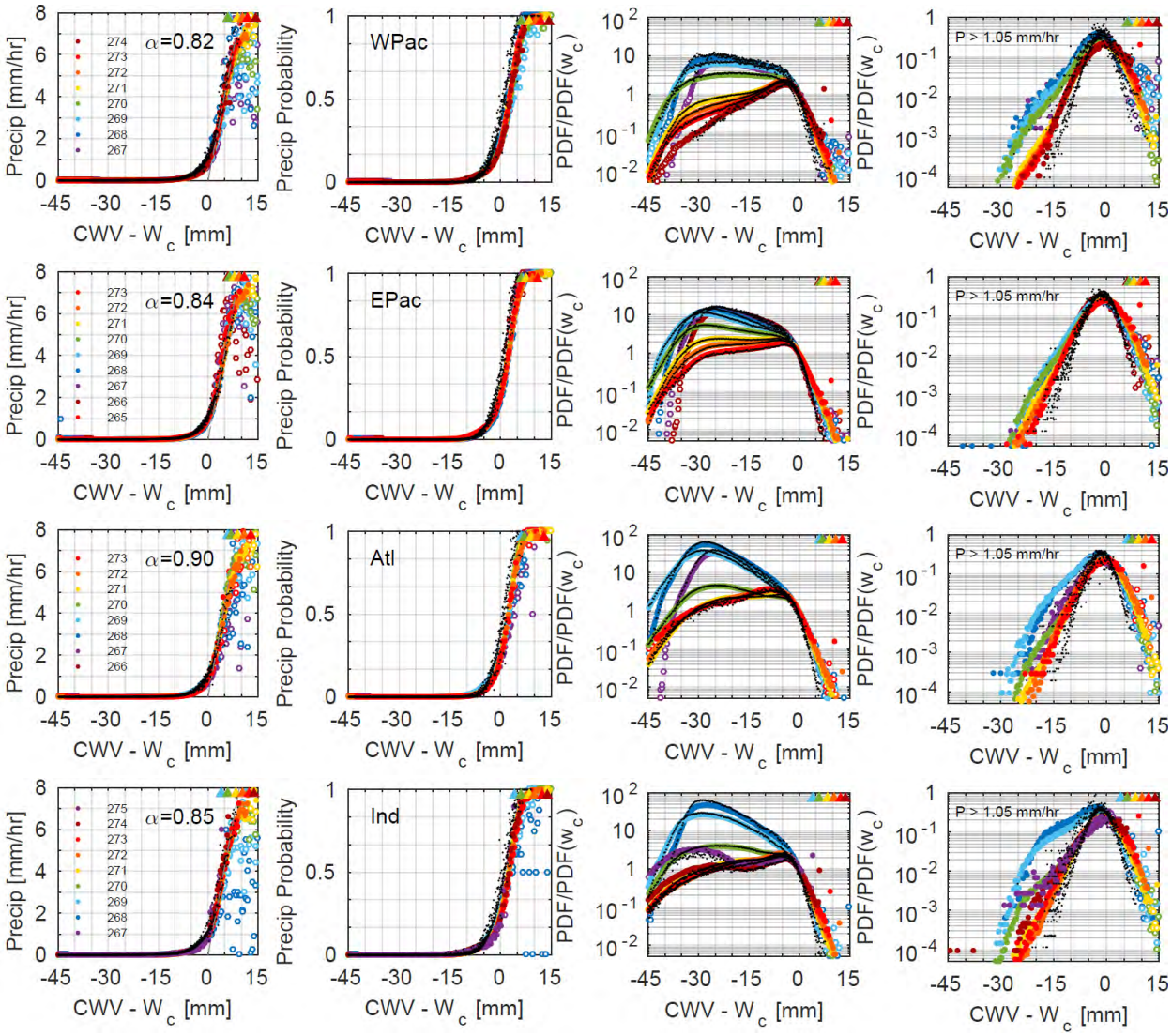

Figure S9: Convective transition statistics as in Fig. S5 for 0.25° (colored markers) and 1.5° (black dots), both with CWV gap-filled using Max.

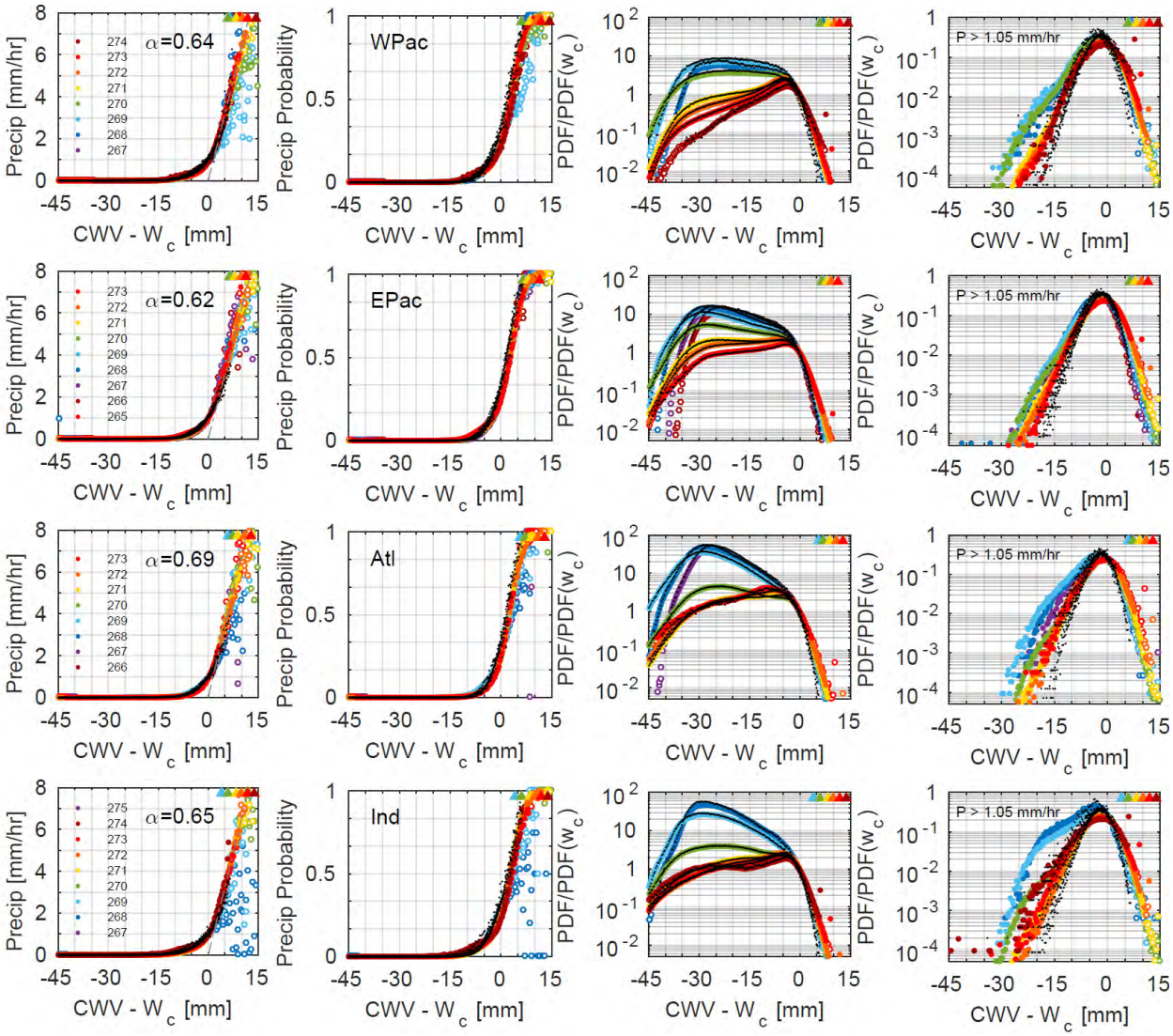

Figure S10: Convective transition statistics as in Fig. S5 for 0.25° (colored markers) and 1° (black dots), both with CWV gap-filled using Nearest.

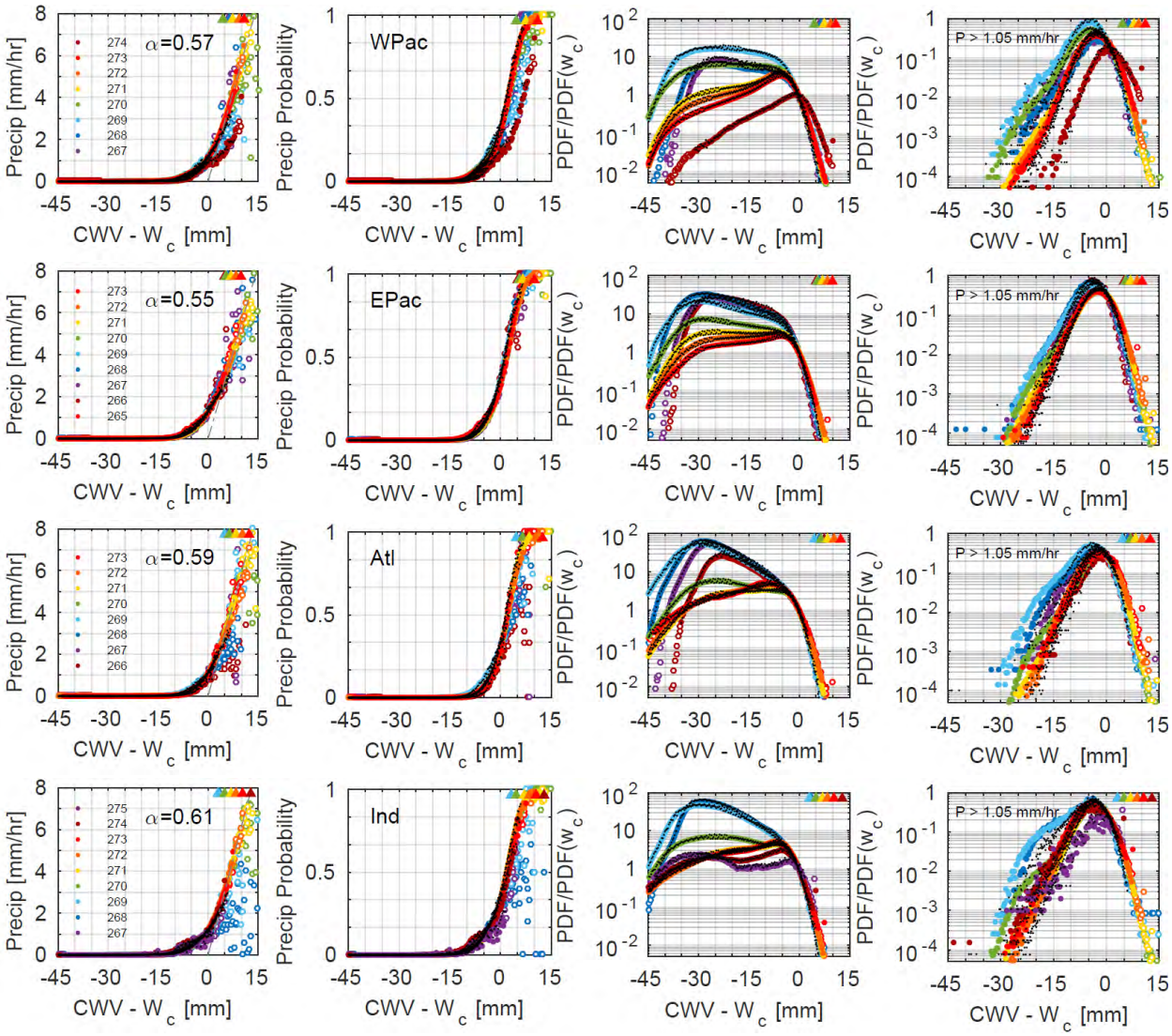

Figure S11: Convective transition statistics as in Fig. S5 for 0.25° (colored markers) and 0.5° (black dots), both with CWV gap-filled using Mean. The 274-K $\hat{T}$-bin for WPac requires the additional effort of choosing a larger P_r to collapse the statistics, which is not done here for illustration purpose (Section S3).

S5. Joint-PDF of CWV relative to critical and precipitation for different temperature and basin

Figure S12 shows the joint-PDF of CWV relative to critical and precipitation rate given different $\widehat{q_{sat}}$ bins and tropical ocean basins. Note that the 70-mm panel for the tropical western Pacific (WPac) is identical to Fig. 7a in the main text. These joint-PDFs are similar across the most common range of $\widehat{q_{sat}}$ and basins.

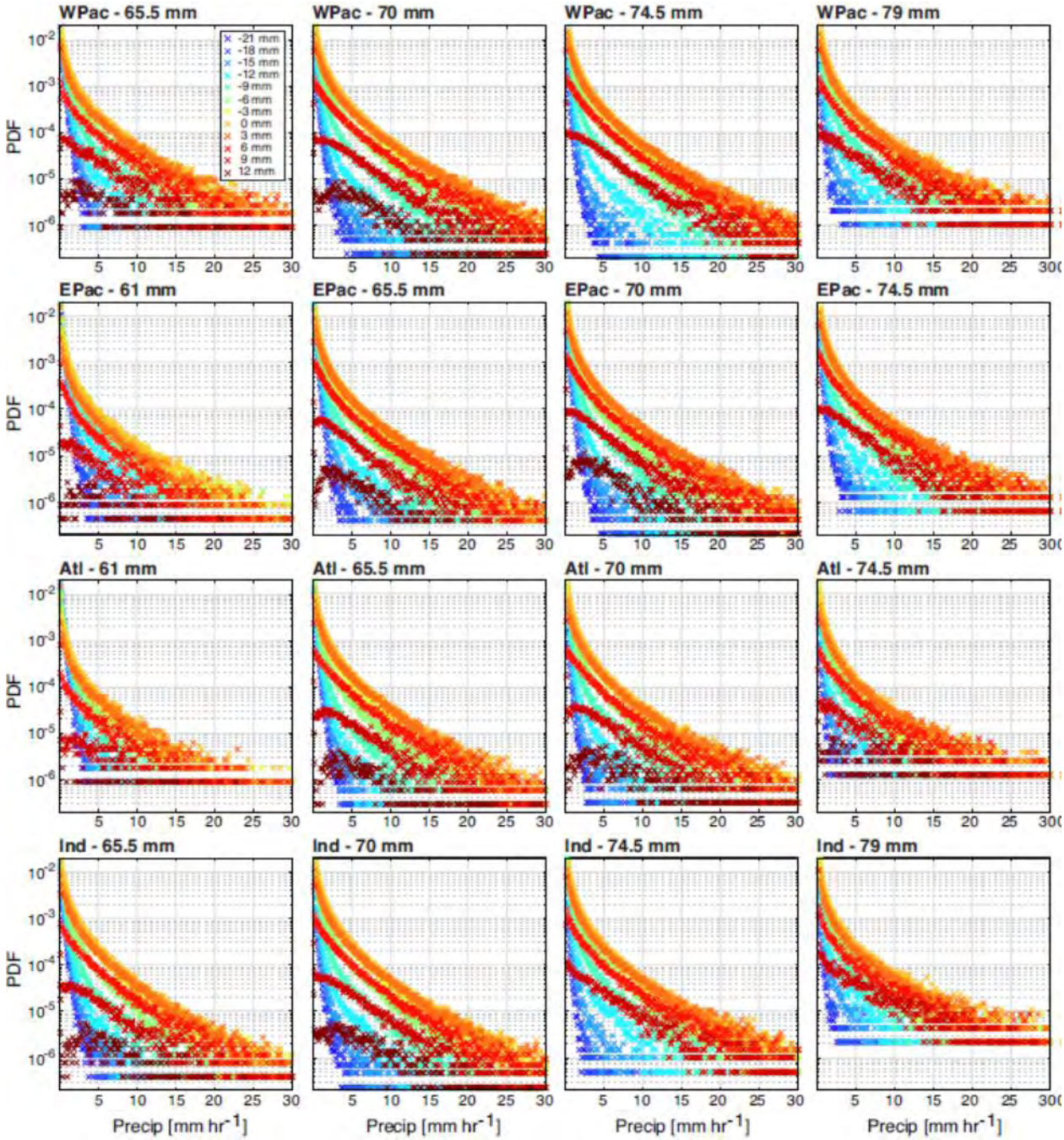

Figure S12: Joint-PDF of CWV relative to critical (colors) and precipitation rate for the four most probable $\widehat{q_{sat}}$ bins for each tropical ocean basin. The joint-PDF is normalized for each $\widehat{q_{sat}}$.

S6. Geographic distribution of bulk tropospheric temperature

Figure S13 shows the probability of occurrences of $\hat{T}$ (bin-width 1 K) as a function of geographical location. The most probable $\hat{T}$-bin is 271 K in all tropical ocean basins but the tropical western Pacific, where the most probable $\hat{T}$ is 272 K. Events with $\hat{T}$ lower than 270 K mostly occur at latitudes around or higher than 20°, but occasionally in the tropical eastern Pacific and Atlantic. These cold events in the tropics, judged from their geographical distribution, are likely due to systems from the extratropics. Some of the coldest and warmest events in the tropics tend to happen near the south Asian continent in the Bay of Bengal and Arabian Sea, likely caused by the circulation pattern driven by the local land-sea contrast.

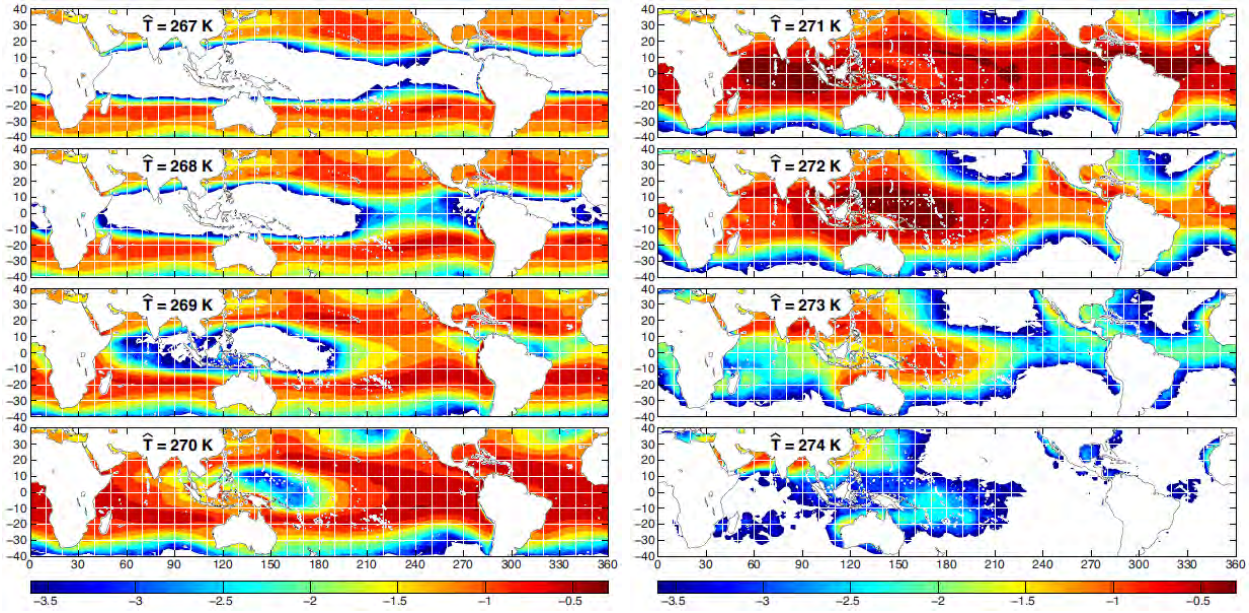

Figure S13: PDF of $\hat{T}$ on a $\log_{10}$-scale as a function of geographical location calculated using Reanalysis-2 temperature for the period of 1 June 2002 – 31 May 2014. The color advances whenever the PDF doubles ($10^{0.3}$ ~ 2). The sum of the PDFs over all $\hat{T}$ (including < 267 K and > 274 K) equals one.

S7. CWV relative to critical as an indicator of precipitation

Section 4 (with Fig. 5) in the main text discusses how CWV relative to critical can be used as an indicator of precipitation. This section provides additional information complementing that discussion. Note that the geographical patterns (not the magnitudes) in Figs. 5 and S14 are robust to the CWV offset and precipitation threshold.

Figure S14a shows the probability of CWV exceeding critical (offset by -1.5 mm; to be consistent with Fig. 5), exhibiting a geographical pattern similar to that of the probability of precipitation (Fig. 5a) and precipitation climatology (Fig. S14b). The most outstanding feature here is the sharp contrast between the major convergence zones and other regions. Note that the corresponding CWV climatology in Fig. S14c, without taking into account the dependence of the critical CWV on temperature, reveals a gentler spatial variation, although the overall pattern still resembles that of precipitation.

While it has been demonstrated that CWV relative to critical is a useful proxy for precipitation, given that the chances of CWV exceeding critical are low (~ 25% in the major convergence zones as in Fig. S14a), and that there are below-critical precipitating events, the contribution of above-critical events to the overall precipitation still has to be quantified. Figure S14d shows the conditional probability of CWV exceeding critical given precipitation, which exhibits a geographical pattern and magnitude similar to the fraction of total precipitation from above-critical events shown in Fig. 5e. In most places in the tropics,

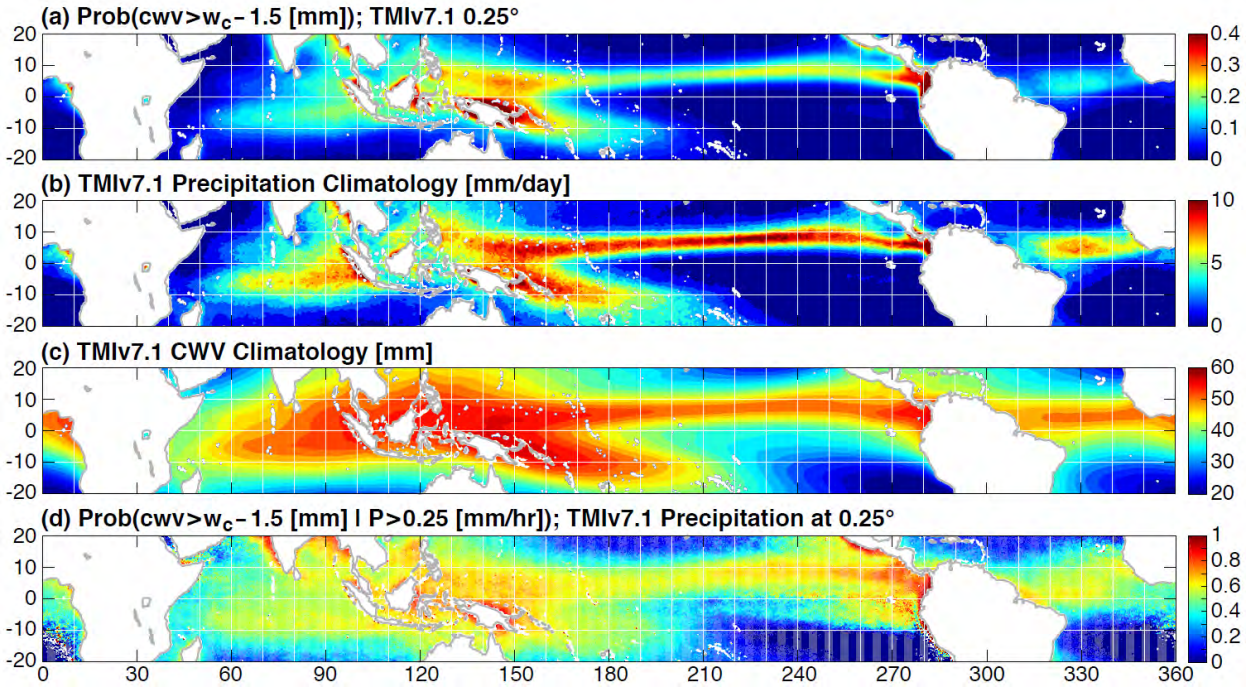

Figure S14: (a) The probability of CWV exceeding critical (offset by -1.5 mm) as a function of geographical location, calculated using TMIv7.1 CWV and Reanalysis-2 temperature. (b) The precipitation climatology calculated using TMIv7.1 precipitation. (c) Same as in (b) but for CWV. (d) The conditional probability [$Prob(cwv > w_c - 1.5\ mm|P > 0.25\ mm\ hr^{-1})$] calculated using TMIv7.1 data and Reanalysis-2 temperature. Here, (a)-(s) are for the same period 01 Jun 2002 – 31 May 2014 and resolution 0.25°, and the critical CWV $w_c(\widehat{q_{sat}})$ is as in Fig. 3 (top center; in the main text) averaged over four basins.

the conditional probability and fraction are higher than 60%, indicating that above-critical events are indeed the major contributor to precipitation. The spatial pattern, when compared to that of the precipitation climatology, shows much weaker spatial contrast, and seems capable of capturing the seasonal shift of precipitation. For instance, one may notice the high values in Figs. S14d and 5e in the tropical eastern Pacific between 0° and 10°S, reflecting the occurrences of deep convective events in this region during the boreal spring (not shown). Since these events are rare, they barely make a dent in Figs. S14a and S14b (255°-275°).

Figure 5f in the main text demonstrates a potential application of using CWV relative to critical as a predictor of precipitation. The false positive rate of this (i.e., the conditional probability of no precipitation given CWV exceeding critical) is given by the conditional probability shown in Figs. 5b, 5c, and 5d (more precisely, one minus the conditional probability), and varies weakly with geographical location. The actual magnitude of the false positive rate depends on the spatial-temporal resolution of precipitation in which one is interested, as well as the CWV offset and precipitation threshold. The false negative rate (the chances of having precipitation given CWV below critical) is given by (one minus) the conditional probability in Fig. S14d. While the exact magnitude of the false negative rate depends on the resolution, CWV offset, and precipitation threshold, it is expected to be lower than 40% in regions including the major convergence zones based on Fig. S14d. There are regions with high false negative rates, but mostly inside regions with climatologically low precipitation.

S8. Low bias of conditional precipitation associated with ground-based CWV measurements

In Fig. 3 of the main text, the conditional precipitation and probability of precipitation compiled using the ARM site data from Manus and Nauru show significant low bias for the highest CWV bins (relative to critical; $cwv - w_c$ > 5 mm) compared to those from the satellite retrievals. To test whether the bias results from the "wet-window" problem associated with the ground-based MWR CWV measurements, Fig. S15 shows the conditional precipitation and conditional probability as in Figs. 3a-3b, but with the ground-based precipitation at Manus and Nauru being replaced by 3B42 precipitation around the 2 islands (a 2.25°x2.25°-average). Since the ground-based data and 3B42 have different temporal frequency/averaging, the necessary interpolation/matching has been performed. In Fig. S15, the low bias for the statistics for Manus and Nauru persists.

An additional combination of TMIv7.1 CWV and 3B42 precipitation gives results quantitatively similar to those shown in Figs. 1-3, except for the slope of the precipitation pickup is slightly smaller (not shown), with no signs the low bias for the highest CWV bins. Given this, and the low bias for Manus and Nauru in Figs. 3 and S15, we conclude that this bias must be caused by the ground-based CWV measurements, and very likely, the "wet-window" problem. Specifically, high CWV events (relative to

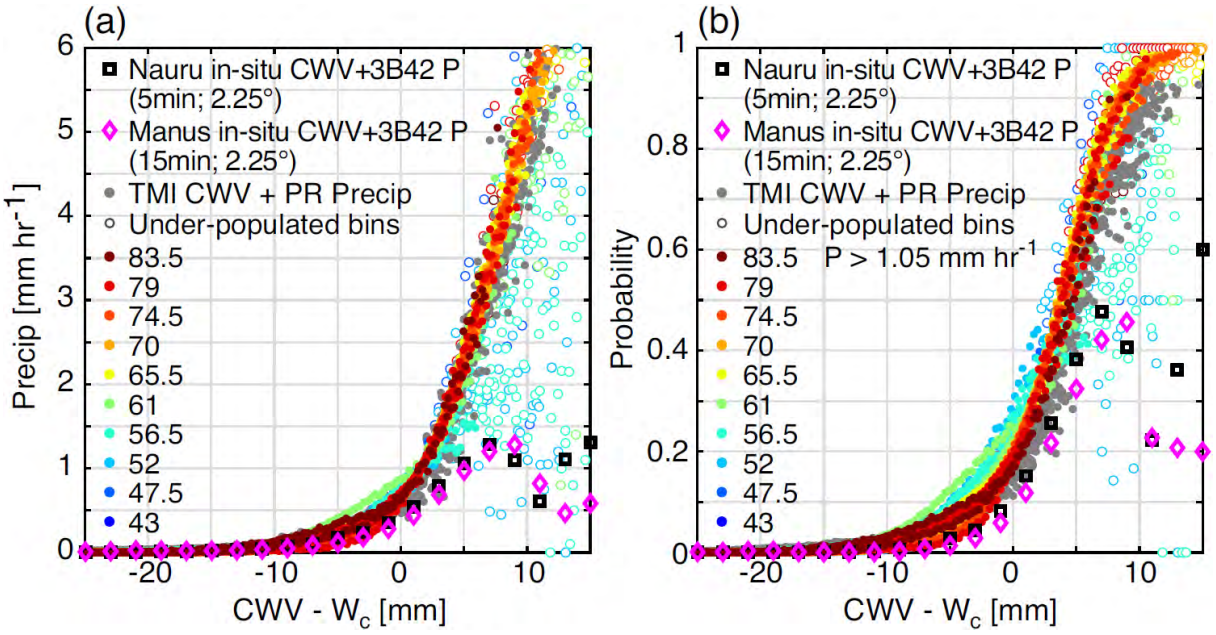

Figure S15: Similar to Fig. 3 of the main text but with the ground-based precipitation from the Manus and Nauru ARM sites replaced by the TRMM 3B42 precipitation averaged around the sites (2.25° x 2.25°). (Left) Collapsed conditional precipitation complied using different datasets, including (i) TMIv7.1 CWV and precipitation (colored dots) with underpopulated bins plotted as open circles, (ii) TMIv7.1 CWV and PR 2A25 precipitation (gray dots) excluding underpopulated bins, and (iii) ARM site CWV and 3B42 precipitation (2.25°-averaged) for Manus (diamonds) and Nauru (squares) Islands in the tropical western Pacific (WPac). Reanalysis-2 temperature is used for (i)-(iii). For (i) and (ii), bins from all four basins are plotted, with data at 0.25° resolution for 01 Jun 2002 – 31 May 2014 and coastal regions excluded. For (iii), the curves are shifted by the corresponding w_c given the temperature ($\widehat{q_{sat}}$ or $\hat{T}$) time series according the w_c-temperature relation for WPac. (Right) Same as in the left panel, but for conditional probability of precipitation defined by P > 1.05 mm hr^{-1}.

critical) with strong precipitation are missing from the CWV timeseries, and the gap-filling, through interpolation, assigns to these events CWV values lower than that happened, while high CWV events associated with weak/no precipitation are not affected as much, resulting in the low bias for the highest $cwv - w_c$ bins. The results here further suggest (i) the adopted gap-filling for ground-based CWV time series cannot satisfactorily restore the missing information; (ii) for $cwv - w_c$ > 5 mm, the CWV data is no longer trustworthy, and (iii) the temperature dependence of critical must be considered in determining this trustworthiness.

References

Sahany, S., J. D. Neelin, K. Hales, and R. B. Neale, 2014: Deep convective transition characteristics in the Community Climate System Model and changes under global warming. *J. Climate,* **27**(24), 9214-9232.

Wentz, F.J., C. Gentemann, K.A. Hilburn, 2015: Remote Sensing Systems TRMM TMI Daily Environmental Suite on 0.25 deg grid, Version 7.1. Remote Sensing Systems, Santa Rosa, CA. Available online at www.remss.com/missions/tmi. Accessed 08 Jul 2016.

Yano, J.-I., C. Liu, and M. W. Moncrieff, 2012: Self-organized criticality and homeostasis in atmospheric convective organization. *J. Atmos. Sci.*, **69**, 3449-3462, doi:10.1175/JAS-D-12-069.1.